Available online at www.sciencedirect.com
SCIENCE DIRECT®
Journal of Computational Physics 207 (2005) 52–68
JOURNAL OF COMPUTATIONAL PHYSICS
www.elsevier.com/locate/jcp

A new paradigm for solving Navier–Stokes equations: streamfunction–velocity formulation

Murli M. Gupta [a,*], Jiten C. Kalita [b]

[a] *Department of Mathematics, The George Washington University, 1922 F Street, NW, Old Main 109D, Washington, DC 20052, USA*
[b] *Department of Mathematics, Indian Institute of Technology, Guwahati 781 039, India*

Received 5 October 2004; received in revised form 4 January 2005; accepted 4 January 2005
Available online 9 February 2005

Abstract

In this paper, we propose a new paradigm for solving Navier–Stokes equations. The proposed methodology is based on a streamfunction–velocity formulation of the two-dimensional steady-state Navier–Stokes equations representing incompressible fluid flows in two-dimensional domains. Similar formulations are also possible for three-dimensional fluid flows. The main advantage of our formulation is that it avoids the difficulties associated with the computation of vorticity values, especially on solid boundaries, encountered when solving the streamfunction–vorticity formulations. Our formulation also avoids the difficulties associated with solving pressure equations of the conventional velocity–pressure formulations of the Navier–Stokes equations.

We describe the new formulation of the Navier–Stokes equations and use this formulation to solve a couple of fluid flow problems. We use a biconjugate gradient method to obtain the numerical solutions of the fluid flow problems and provide detailed comparison data for the lid driven cavity flow problem. It is discovered that our new formulation successfully provides high accuracy solutions for the benchmark problem. In addition, we also solve a problem of flow in a rectangular cavity with aspect ratio 2 and compare our results qualitatively and quantitatively with numerical and experimental results available in the literature. In all cases, we obtain high accuracy solutions with little additional cost.

PACS: 02.60.Cb; 47.11.+j; 02.70.Bf

Keywords: Streamfunction–velocity formulation; Navier–Stokes equations; Biharmonic equation; High accuracy; Compact approximations; Finite differences

* Corresponding author. Tel.: +1 202 994 4857; fax: +1 202 994 6760.
E-mail addresses: mmg@gwu.edu (M.M. Gupta), jiten@iitg.ernet.in (J.C. Kalita).

0021-9991/$ - see front matter
doi:10.1016/j.jcp.2005.01.002

1. Introduction

Consider the two-dimensional incompressible Navier–Stokes equations in the traditional primitive variable (velocity–pressure) formulation:

$$u_t + uu_x + vu_y = -p_x + v(u_{xx} + u_{yy}), \tag{1}$$

$$v_t + uv_x + vv_y = -p_y + v(v_{xx} + v_{yy}), \tag{2}$$

$$u_x + v_y = 0. \tag{3}$$

Though this formulation accurately represents the fluid flow phenomena, its direct solution traditionally has been difficult to obtain due to the pressure term in Eqs. (1) and (2). Partly in order to avoid handling the pressure variable, an alternative formulation using streamfunction and vorticity has been used for several decades. The alternative formulation introduces the streamfunction ψ and vorticity ω:

$$\psi_{xx} + \psi_{yy} = -\omega(x,y), \tag{4}$$

$$\omega_t + (u\omega_x + v\omega_y) = \frac{1}{Re}(\omega_{xx} + \omega_{yy}), \tag{5}$$

where $(x,y) \in \Omega$, Re is the non-dimensional Reynolds number; the velocity components are defined as

$$u(x,y) = \psi_y, \quad v(x,y) = -\psi_x. \tag{6}$$

This formulation has been very successful and has been used by a large number of researchers over the past several decades to test new methods for the numerical solutions of a variety of fluid flow problems. Typical difficulty with this formulation consists in the specification of vorticity values at the no-slip boundaries; the vorticity ω is defined through the Poisson equation $-\omega = \psi_{xx} + \psi_{yy}$ which needs to be solved discretely on the boundaries so that boundary values of the vorticity can be specified for the vorticity transport equation when this formulation is utilized. However, the values of vorticity ω on the boundaries are generally unspecified and one has to carry out a variety of numerical approximations in order to specify the boundary values of vorticity.

In this paper, we propose the following finite difference formulation for solving the steady-state Navier–Stokes equations. The discretization is carried out on a uniform grid of width h in both x and y directions and the approximation at a grid point (x,y) utilizes the values of ψ at the eight nearest neighbors of (x,y) in the compact stencil, and the values of velocities u,v at the nearest neighbors

$$\begin{aligned}
&-28\psi(x,y) + 8[\psi(x+h,y) + \psi(x-h,y) + \psi(x,y+h) + \psi(x,y-h)] - [\psi(x+h,y+h) \\
&+ \psi(x-h,y+h) + \psi(x-h,y-h) + \psi(x+h,y-h)] - 3h[u(x,y+h) - u(x,y-h) - v(x+h,y) \\
&+ v(x-h,y)] - \frac{Reh}{4}u(x,y)[2(\psi(x+h,y) - \psi(x-h,y)) - \psi(x+h,y+h) + \psi(x-h,y+h) \\
&+ \psi(x-h,y-h) - \psi(x+h,y-h) + 2h(v(x+h,y) - 2v(x,y) + v(x-h,y))] \\
&- \frac{Reh}{4}v(x,y)[2(\psi(x,y+h) - \psi(x,y-h)) - \psi(x+h,y+h) - \psi(x-h,y+h) \\
&+ \psi(x-h,y-h) + \psi(x+h,y-h) - 2h(u(x,y+h) - 2u(x,y) + u(x,y-h))] = 0.
\end{aligned} \tag{7}$$

The velocities at a point (x,y) may be approximated as follow:

$$u(x,y) = \frac{3}{4h}[\psi(x,y+h) - \psi(x,y-h)] - \frac{1}{4}[u(x,y+h) + u(x,y-h)], \tag{8}$$

$$v(x,y) = -\frac{3}{4h}[\psi(x+h,y) - \psi(x-h,y)] - \frac{1}{4}[v(x+h,y) + v(x-h,y)]. \tag{9}$$

The origins and history of this finite difference approximation are described in the following section of this paper. This approximation has a truncation error of order $O(h^2)$. We use this approximation to solve two fluid flow problems: the benchmark problem of incompressible fluid flow in a lid driven square cavity which is solved for Reynolds numbers as high as 10,000, and a problem of flow in a lid driven rectangular cavity with an aspect ratio of 2. In each case, we obtain solutions that agree very well, both qualitatively and quantitatively, with published results.

2. Biharmonic equation and origins of the streamfunction–velocity formulation

Consider the Dirichlet problem for the biharmonic equation:

$$\frac{\partial^4\phi}{\partial x^4} + 2\frac{\partial^4\phi}{\partial x^2\partial y^2} + \frac{\partial^4\phi}{\partial y^4} = f(x,y), \quad (x,y) \in \Omega, \tag{10}$$

$$\phi = g_1(x,y), \quad \frac{\partial\phi}{\partial n} = g_2(x,y) \qquad (x,y) \in \partial\Omega, \tag{11}$$

where Ω is a closed convex domain in two dimensions and $\partial\Omega$ is its boundary.

Various approaches for the numerical solution of the boundary value problem (10) have been considered in the literature [1,7–9,13,18]. A popular technique is to split it into two coupled Poisson equations for ϕ and ξ:

$$\frac{\partial^2\phi}{\partial x^2} + \frac{\partial^2\phi}{\partial y^2} = \xi, \tag{12}$$

$$\frac{\partial^2\xi}{\partial x^2} + \frac{\partial^2\xi}{\partial y^2} = f. \tag{13}$$

Each of these Poisson equations may be discretized using the standard five point approximations and solved using fast Poisson solvers. The difficulty with this approach is that the boundary conditions for the new variable ξ are undefined and need to be approximated from the discrete form of Eq. (12). The coupled equation approach has been used by many authors (see [7,8] and other references for detailed background).

Another traditional approach for solving the biharmonic equations is to discretize the biharmonic equation (Eq. 10) on a uniform grid using a 13 point approximation with truncation error of order h^2 or using a 25 point approximation with truncation error of order h^4. The thirteen point approximation of the biharmonic equation at a grid point (x_i,y_j) may be written as

$$\begin{aligned} &20\phi_{i,j} - 8[\phi_{i+1,j} + \phi_{i,j+1} + \phi_{i-1,j} + \phi_{i,j-1}] + 2[\phi_{i+1,j+1} + \phi_{i-1,j+1} + \phi_{i-1,j-1} + \phi_{i+1,j-1}] \\ &+ (\phi_{i+2,j} + \phi_{i,j+2} + \phi_{i-2,j} + \phi_{i,j-2}) = h^4 f_{i,j}. \end{aligned} \tag{14}$$

This approximation connects the values of $\phi_{i,j}$ in terms of 12 neighboring values of ϕ. The above difference approximation needs to be modified at grid points near the boundaries. Many such modifications were discussed in [9]. There are further difficulties with the solution of the linear systems obtained through the thirteen point discretization of the biharmonic equation. The direct solvers for solving the resulting systems of linear equations can only be used for moderate values of grid width h [9] and the conventional iterative methods such as Jacobi or Gauss–Seidel [14,15] either converge very slowly or diverge.

Certain second and fourth order compact finite difference approximations for the biharmonic equation (Eq. 10) on a 9 point cell have been known for some time (see, e.g. [1,13,18]). The compact approach involves discretizing the biharmonic equation using not just the grid values of the unknown solution ϕ but also the values of the gradients ϕ_x, and ϕ_y at selected grid points. As described in detail in [1], this approach is advantageous because:

(i) the given boundary conditions are exactly satisfied and no further approximations need to be carried out at the boundaries;
(ii) the proposed finite difference approximations are defined on a 9 point compact cell and no special adjustments are needed at grid points close to the boundaries;
(iii) values of the gradients ϕ_x and ϕ_y are already computed and available at all grid points and need not be further approximated from the computed values of the solution ϕ.

The second order compact scheme for the biharmonic equation (Eq. 10) is given by

$$28\phi_{i,j} - 8[\phi_{i+1,j} + \phi_{i,j+1} + \phi_{i-1,j} + \phi_{i,j-1}] + [\phi_{i+1,j+1} + \phi_{i-1,j+1} + \phi_{i-1,j-1} + \phi_{i+1,j-1}] + 3h[(\phi_x)_{i+1,j} - (\phi_x)_{i-1,j} + (\phi_y)_{i,j+1} - (\phi_y)_{i,j-1}] = \frac{h^4}{2} f_{i,j}. \tag{15}$$

This scheme discretizes two-dimensional biharmonic equations at a grid point (x_i,y_j) using the eight neighboring values of ϕ, two values of ϕ_x and two values of ϕ_y. Truncation error of this approximation is of order h^2; this finite difference scheme was obtained by employing the symbolic algebra package *Mathematica* [1].

Compatible approximations for ϕ_x and ϕ_y can also be obtained. The well known central difference approximations of second order accuracy may be used:

$$(\phi_x)_{i,j} = \frac{(\phi_{i+1,j} - \phi_{i-1,j})}{2h}, \tag{16}$$

$$(\phi_y)_{i,j} = \frac{(\phi_{i,j+1} - \phi_{i,j-1})}{2h}. \tag{17}$$

Another alternative is to use the fourth order approximations for ϕ_x and ϕ_y:

$$(\phi_x)_{i,j} = \frac{3}{4h}(\phi_{i+1,j} - \phi_{i-1,j}) - \frac{1}{4}\Big((\phi_x)_{i+1,j} + (\phi_x)_{i-1,j}\Big), \tag{18}$$

$$(\phi_y)_{i,j} = \frac{3}{4h}(\phi_{i,j+1} - \phi_{i,j-1}) - \frac{1}{4}\Big((\phi_y)_{i,j+1} + (\phi_y)_{i,j-1}\Big). \tag{19}$$

A fourth order compact scheme for the biharmonic equation is also available. This scheme uses, at a grid point (x_i,y_j), the eight neighboring values of ϕ in the compact cell and six values each of ϕ_x and ϕ_y. This approximation also uses the values of the forcing function $f(x,y)$ at four neighboring points. Truncation error of the following approximation is of order h^4

$$\begin{aligned}\phi_{i,j} &- \frac{3}{11}\left[\phi_{i+1,j} + \phi_{i,j+1} + \phi_{i-1,j} + \phi_{i,j-1}\right] + \frac{1}{44}\left[\phi_{i+1,j+1} + \phi_{i-1,j+1} + \phi_{i-1,j-1} + \phi_{i+1,j-1}\right] \\ &+ \frac{7h}{66}\left[(\phi_x)_{i+1,j} - (\phi_x)_{i-1,j} + (\phi_y)_{i,j+1} - (\phi_y)_{i,j-1}\right] + \frac{h}{264}\left[(\phi_x)_{i+1,j+1} - (\phi_x)_{i-1,j+1} - (\phi_x)_{i-1,j-1}\right. \\ &\left.+(\phi_x)_{i+1,j-1} + (\phi_y)_{i+1,j+1} + (\phi_y)_{i-1,j+1} - (\phi_y)_{i-1,j-1} - (\phi_y)_{i+1,j-1}\right] \\ &= \frac{h^4}{792}\left[11 f_{i,j} + (f_{i+1,j} + f_{i,j+1} + f_{i-1,j} + f_{i,j-1})\right].\end{aligned} \tag{20}$$

Compatible fourth order approximations for ϕ_x and ϕ_y are given above.

The approximations for the two-dimensional biharmonic equation were obtained using a *Mathematica* code presented in [1]. Our two-dimensional code was subsequently extended to three-dimensional biharmonic equations in [2] to obtain a family of finite difference approximations on the 27 point compact cubic cell.

For the present work, we extended the *Mathematica* code for the two-dimensional biharmonic equation to obtain similar compact schemes for the Navier–Stokes equations. In order to accomplish this goal, we transformed the streamfunction–vorticity form of the steady-state Navier–Stokes equations into a fourth order partial differential equation

$$\frac{\partial^4\psi}{\partial x^4}+2\frac{\partial^4\psi}{\partial x^2\partial y^2}+\frac{\partial^4\psi}{\partial y^4}-Re\,u\left[\frac{\partial^3\psi}{\partial x^3}+\frac{\partial^3\psi}{\partial x\partial y^2}\right]-Re\,v\left[\frac{\partial^3\psi}{\partial x^2\partial y}+\frac{\partial^3\psi}{\partial y^3}\right]=0. \tag{21}$$

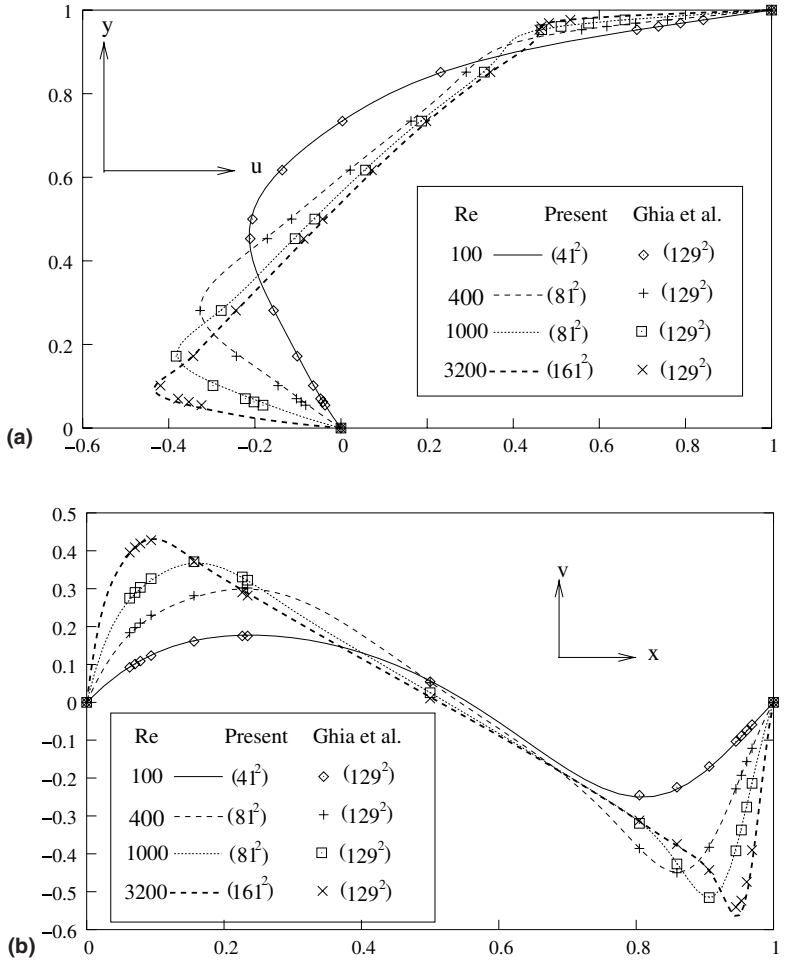

Fig. 1. Comparisons of (a) horizontal velocity along the vertical centerline and (b) vertical velocity along the horizontal centerline for the lid-driven square cavity flows from $Re = 100$ to $Re = 3200$.

For the purpose of deriving the compact difference schemes for This equation, we treat the velocities u and v in the above equation as locally fixed at the grid point (x,y). Our *Mathematica* code produces the following finite difference scheme for the Navier–Stokes equations; truncation error of this scheme is of order h^2

$$\begin{aligned}
&-28\psi(x,y)+8[\psi(x+h,y)+\psi(x-h,y)+\psi(x,y+h)+\psi(x,y-h)]-[\psi(x+h,y+h)\\
&+\psi(x-h,y+h)+\psi(x-h,y-h)+\psi(x+h,y-h)]-3h[u(x,y+h)-u(x,y-h)-v(x+h,y)\\
&+v(x-h,y)]-\frac{Reh}{4}u(x,y)[2(\psi(x+h,y)-\psi(x-h,y))-\psi(x+h,y+h)+\psi(x-h,y+h)\\
&+\psi(x-h,y-h)-\psi(x+h,y-h)+2h(v(x+h,y)-2v(x,y)+v(x-h,y))]\\
&-\frac{Reh}{4}v(x,y)[2(\psi(x,y+h)-\psi(x,y-h))-\psi(x+h,y+h)-\psi(x-h,y+h)\\
&+\psi(x-h,y-h)+\psi(x+h,y-h)-2h(u(x,y+h)-2u(x,y)+u(x,y-h))]=0. \qquad (22)
\end{aligned}$$

We have also derived a fourth order compact scheme for Navier–Stokes equations in streamfunction–velocity variables and details of this scheme will be reported in future.

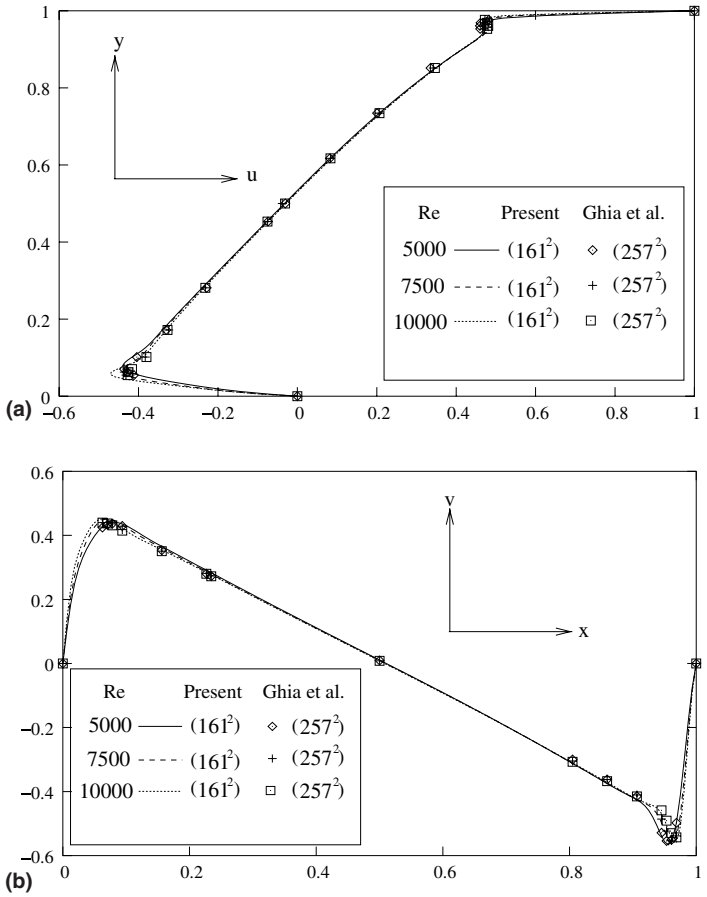

Fig. 2. Comparisons of (a) horizontal velocity along the vertical centerline and (b) vertical velocity along the horizontal centerline for the lid-driven square cavity flows from $Re = 5000$ to $Re = 10{,}000$.

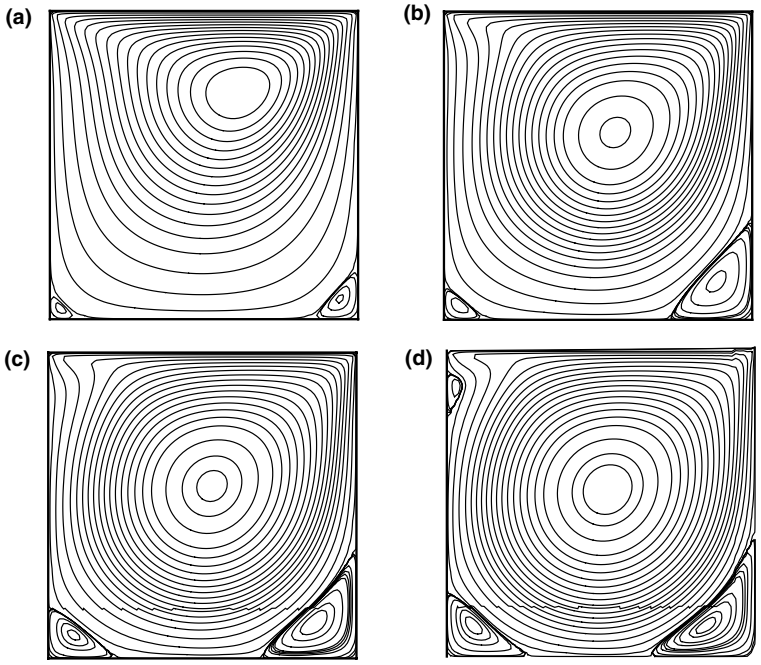

Fig. 3. Streamfunction contours for the lid-driven square cavity flows for (a) $Re = 100$, (b) $Re = 400$, (c) $Re = 1000$ and (d) $Re = 2000$ (all computations obtained with 81×81 grid).

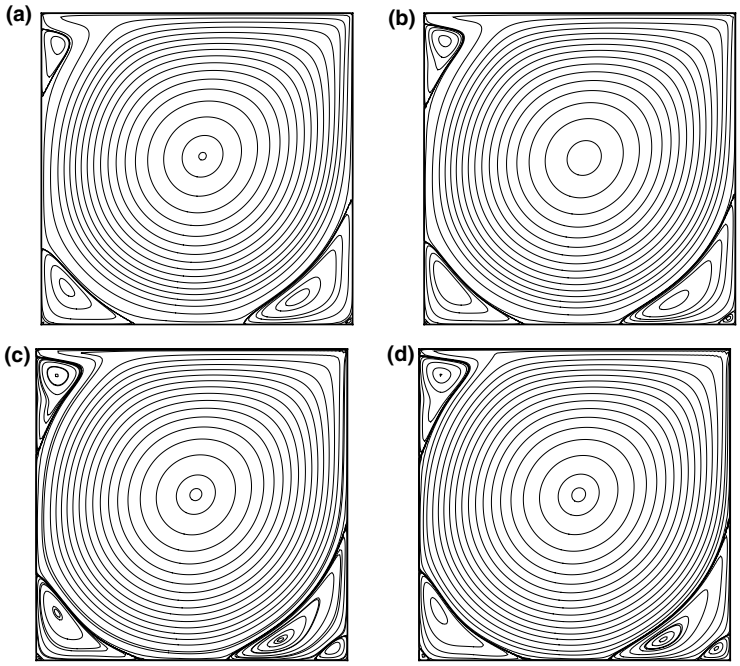

Fig. 4. Streamfunction contours for the lid-driven square cavity flows for (a) $Re = 3200$, (b) $Re = 5000$, (c) $Re = 7500$ and (d) $Re = 10{,}000$ (all computations obtained with 161×161 grid).

3. Solution of algebraic systems

We now discuss the solution of algebraic systems associated with the newly proposed finite difference approximations. The finite difference approximation given in Eqs. (7)–(9) may be rewritten as follows:

$$\begin{aligned}&\psi_{i-1,j-1} - 8\psi_{i,j-1} + \psi_{i+1,j-1} - 8\psi_{i-1,j} + 28\psi_{i,j} - 8\psi_{i+1,j} + \psi_{i-1,j+1} - 8\psi_{i,j+1} + \psi_{i+1,j+1}\\ &\quad - 3h\left(u_{i,j-1} - u_{i,j+1} + v_{i+1,j} - v_{i-1,j}\right) - 0.5Re\,h^2\left\{v_{i,j}\left(u_{i+1,j} + u_{i-1,j} + u_{i,j+1} + u_{i,j-1}\right)\right.\\ &\quad \left. - u_{i,j}\left(v_{i+1,j} + v_{i-1,j} + v_{i,j+1} + v_{i,j-1}\right)\right\} = 0,\end{aligned} \tag{23}$$

$$u_{i,j} = \frac{3}{4h}\left(\psi_{i,j+1} - \psi_{i,j-1}\right) - \frac{1}{4}\left(u_{i,j+1} + u_{i,j-1}\right), \tag{24}$$

$$v_{i,j} = -\frac{3}{4h}\left(\psi_{i+1,j} - \psi_{i-1,j}\right) - \frac{1}{4}\left(v_{i+1,j} + v_{i-1,j}\right). \tag{25}$$

Note that Eq. (23) is derived from Eq. (7) using the definitions of the velocities u and v in Eq. (6) and the approximations in Eqs. (16) and (17). This defines our discrete problems with variables $\psi_{i,j}$, $u_{i,j}$ and $v_{i,j}$ at each point of the discrete region. The system of equations arising from Eq. (23) leads to the following matrix form:

$$A\boldsymbol{\Psi} = \mathbf{f}(\mathbf{Re}, \mathbf{u}, \mathbf{v}), \tag{26}$$

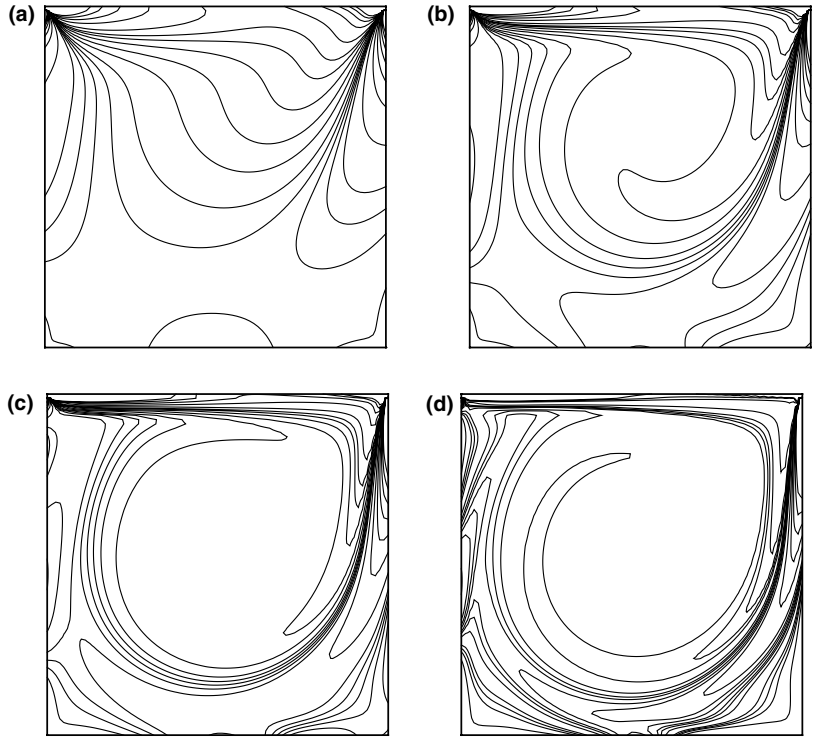

Fig. 5. Post-processed vorticity contours for the lid-driven square cavity flows for (a) $Re = 100$, (b) $Re = 400$, (c) $Re = 1000$ and (d) $Re = 2000$ (all computations obtained with 81×81 grid).

where for a grid of size $m \times n$, the coefficien
ponent vectors. We solve this problem using
we solve Eq. (26) using the biconjugate grad
stitutes inner iterations. Once (26) is solved
(24) and (25). This constitutes one outer iter
the inner as well as the outer iteration cycle
smaller values of λ.

We note that classical iterative methods
equation ($Re = 0$) as seen in [1,2]. We al
[11,15,17,19] method was used for larger
no computational difficulties with the use
in the present study were obtained with
out on a PC with a Pentium 4 processor
the maximum ψ-error between two success
$Re = 100$, we used zero initial data whereas
profile of the previously smaller Re to com

ted
rried
d when
10^{-6}. For
own solution

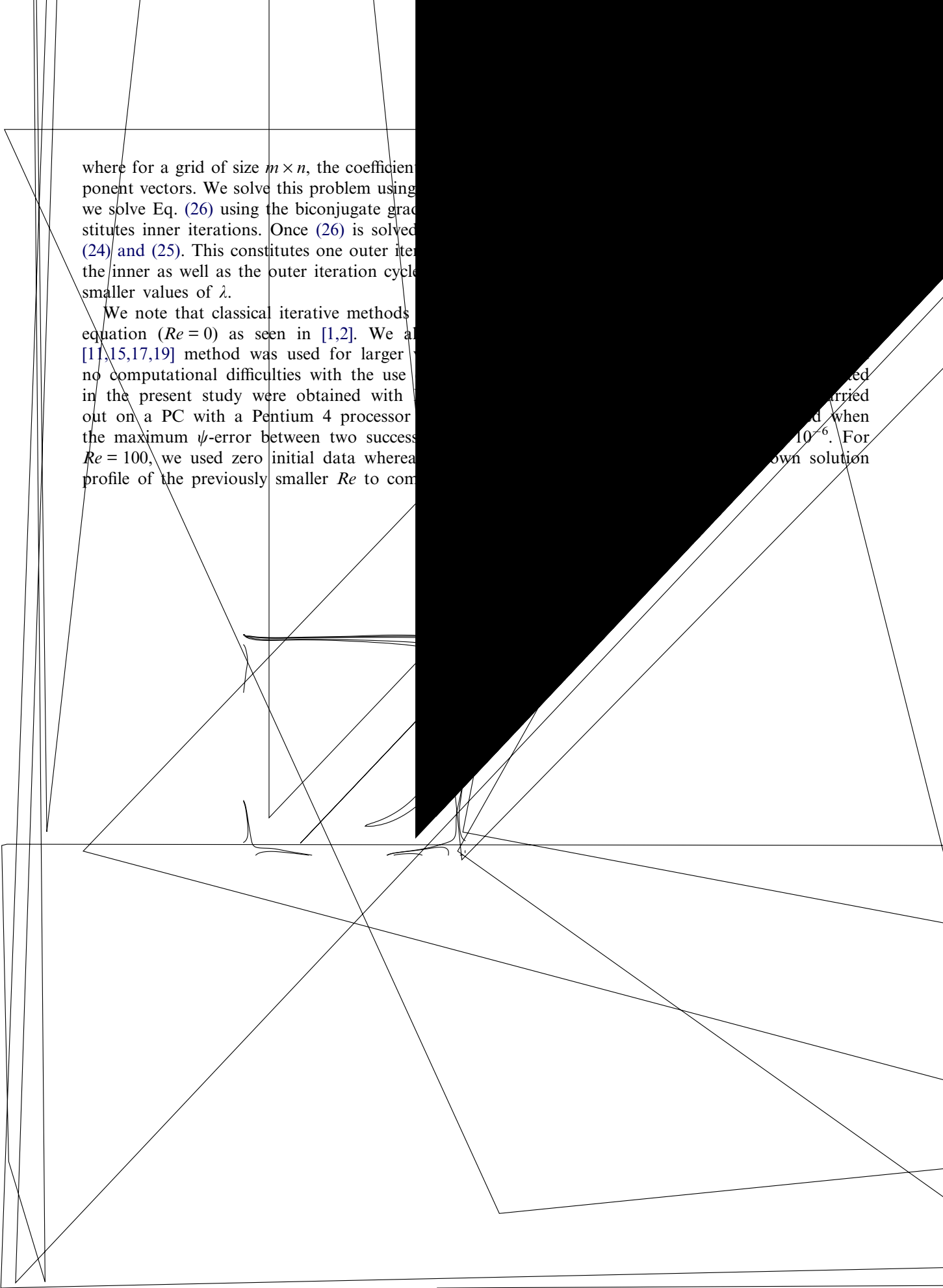

4. Numerical experiments

4.1. Test problem 1

We first consider the problem of two-dimensional lid-driven square cavity flow which is extensively used as a benchmark for code validation of the incompressible N–S equations. The cavity is defined in the square $0 \leqslant x,y \leqslant 1$ and the governing equations are given by the steady-state forms of Eqs. (4) and (5):

Table 1
Strength and location of the centers of primary vortex for the lid-driven square cavity problem

Re		$\psi_{\min}$	x	y
100	[20]	−0.103	0.6188	0.7375
	[6]	−0.103	0.6172	0.7344
	[16]	−0.103	0.6167	0.7417
	[10]	−0.103	0.6196	0.7373
	Present	−0.103	0.6125	0.7375
400	[20]	−0.114	0.5563	0.6000
	[6]	−0.114	0.5547	0.6055
	[16]	−0.113	0.5571	0.6071
	[10]	−0.112	0.5608	0.6078
	Present	−0.113	0.5500	0.6125
1000	[20]	−0.117	0.5438	0.5625
	[6]	−0.118	0.5313	0.5625
	[16]	−0.116	0.5286	0.5643
	[10]	−0.118	0.5333	0.5647
	[4]	−0.119	0.5308	0.5652
	[5]	−0.116	0.5313	0.5586
	Present	−0.117	0.5250	0.5625
2000	[20]	−0.112	0.5250	0.5500
	[10]	−0.120	0.5255	0.5490
	Present	−0.118	0.5250	0.5500
3200	[12]	−0.115	–	–
	[6]	−0.120	0.5165	0.5469
	Present	−0.122	0.5188	0.5438
5000	[20]	−0.092	0.5125	0.5313
	[6]	−0.119	0.5117	0.5352
	[12]	−0.112	–	–
	[5]	−0.114	0.5156	0.5313
	[10]	−0.121	0.5176	0.5373
	[3]	−0.122	0.5113	0.5283
	Present	−0.122	0.5125	0.5375
7500	[6]	−0.120	0.5117	0.5322
	[5]	−0.111	0.5156	0.5234
	[10]	−0.122	0.5176	0.5333
	[3]	−0.122	0.5132	0.5321
	Present	−0.122	0.5125	0.5313
10,000	[6]	−0.120	0.5117	0.5333
	[5]	−0.105	0.5156	0.5234
	[16]	−0.103	0.5140	0.5307
	[3]	−0.122	0.5113	0.5302
	Present	−0.122	0.5125	0.5313

$$\psi_{xx} + \psi_{yy} = -\omega(x, y), \tag{27}$$

$$\omega_{xx} + \omega_{yy} - Re(u\omega_x + v\omega_y) = 0. \tag{28}$$

The fluid motion is generated by the sliding motion of the top wall of the cavity ($y = 1$) in its own plane from left to right. Boundary conditions on the top wall are given as $u = 1$, $v = 0$. On all other walls of the cavity the velocities are zero ($u = v = 0$). Further the streamfunction values on all four walls are zero ($\psi = 0$).

Table 2
Strength and location of the centers of secondary vortex: bottom of the lid-driven square cavity

Re		Bottom left			Bottom right		
		ψ_{max}	x	y	ψ_{max}	x	y
100	[20]	1.94e − 6	0.0375	0.0313	1.14e − 5	0.9375	0.0563
	[6]	1.75e − 6	0.0313	0.0391	1.25e − 5	0.9453	0.0625
	[16]	2.05e − 6	0.0333	0.0250	1.32e − 5	0.9417	0.0500
	[10]	1.72e − 6	0.0392	0.0353	1.22e − 5	0.9451	0.0627
	[5]	1.63e − 6	0.0313	0.0391	1.23e − 5	0.9453	0.0625
	Present	1.83e − 6	0.0375	0.0375	1.45e − 5	0.9375	0.0625
400	[20]	1.46e − 5	0.0500	0.0500	6.45e − 4	0.8875	0.1188
	[6]	1.42e − 5	0.0508	0.0469	6.42e − 4	0.8906	0.1250
	[16]	1.45e − 5	0.0500	0.0429	6.44e − 4	0.8857	0.1143
	[10]	1.30e − 5	0.0549	0.0510	6.19e − 4	0.8902	0.1255
	Present	1.30e − 5	0.0500	0.0500	6.48e − 4	0.8875	0.1250
1000	[20]	2.24e − 4	0.0750	0.0813	1.74e − 3	0.8625	0.1063
	[6]	2.31e − 4	0.0859	0.0781	1.75e − 3	0.8594	0.1094
	[16]	2.17e − 4	0.0857	0.0714	1.70e − 3	0.8643	0.1071
	[10]	2.22e − 4	0.0902	0.0784	1.69e − 3	0.8667	0.1137
	[5]	3.25e − 4	0.0859	0.0820	1.91e − 3	0.8711	0.1094
	[4]	2.33e − 4	0.0833	0.0781	1.73e − 3	0.8640	0.1118
	Present	2.02e − 4	0.0875	0.0750	1.70e − 3	0.8625	0.1125
2000	[20]	6.90e − 4	0.0875	0.1063	2.60e − 3	0.8375	0.0938
	[10]	7.26e − 4	0.0902	0.1059	2.44e − 3	0.8471	0.0980
	Present	8.58e − 4	0.0875	0.1000	2.41e − 3	0.8375	0.1000
3200	[6]	9.78e − 4	0.0859	0.1094	3.14e − 3	0.8125	0.0859
	Present	1.03e − 3	0.0813	0.1188	2.86e − 3	0.8125	0.0875
5000	[20]	1.67e − 3	0.0625	0.1563	5.49e − 3	0.8500	0.0813
	[6]	1.36e − 3	0.0703	0.1367	3.08e − 3	0.8086	0.0742
	[10]	1.35e − 3	0.0784	0.1313	3.03e − 3	0.8078	0.0745
	[5]	2.22e − 3	0.0664	0.1484	4.65e − 3	0.8301	0.0703
	[3]	1.37e − 3	0.0725	0.1370	3.07e − 3	0.8041	0.0725
	Present	1.32e − 3	0.0750	0.1313	2.96e − 3	0.8000	0.0750
7500	[6]	1.47e − 3	0.0645	0.1504	3.28e − 3	0.7813	0.0625
	[10]	1.51e − 3	0.0706	0.1529	3.20e − 3	0.7922	0.0667
	[5]	4.76e − 3	0.0703	0.1289	8.32e − 3	0.8828	0.0820
	[3]	1.53e − 3	0.0642	0.1526	3.23e − 3	0.7900	0.0648
	Present	1.60e − 3	0.0688	0.1500	3.05e − 3	0.7813	0.0625
10,000	[6]	1.52e − 3	0.0586	0.1641	3.42e − 3	0.7656	0.0586
	[5]	6.23e − 3	0.0781	0.1133	9.86e − 3	0.8945	0.0820
	[3]	1.62e − 3	0.0588	0.1623	3.19e − 3	0.7747	0.0588
	Present	1.50e − 3	0.0623	0.1564	3.22e − 3	0.7813	0.0625

Table 3
Strength and location of the centers of secondary vortex: top left side wall of the lid-driven square cavity

Re		ψ_{max}	x	y
2000	Present	1.22e − 4	0.0375	0.8875
3200	[6]	7.28e − 4	0.0547	0.8984
	Present	7.33e − 4	0.0563	0.9000
5000	[6]	1.46e − 3	0.0625	0.9102
	[5]	1.75e − 3	0.0625	0.9102
	[10]	1.40e − 3	0.0667	0.9059
	[3]	1.45e − 3	0.0635	0.9092
	Present	1.54e − 3	0.0688	0.9125
7500	[6]	2.05e − 3	0.0664	0.9141
	[5]	3.14e − 3	0.0664	0.9141
	[10]	2.06e − 3	0.0706	0.9098
	[3]	2.13e − 3	0.0669	0.9116
	Present	2.07e − 3	0.0688	0.9125
10,000	[6]	2.42e − 3	0.0703	0.9141
	[5]	4.03e − 3	0.0664	0.9141
	[3]	2.63e − 3	0.0702	0.9108
	Present	2.50e − 3	0.0688	0.9188

As described in the previous section, we solve Eqs. (23)–(25) to obtain the streamfunction ψ and velocities u and v at each grid point. The vorticity values are determined through post processing using a discretized form of Eq. (27).

In Fig. 1, we present comparisons of the horizontal velocities on the vertical centerline and the vertical velocities on the horizontal centerline of the square cavity for Reynolds numbers ranging from 100 to 3200 and compare our data with that from Ghia et al. [6]. While the data for Ghia et al. [6] was obtained using a 129×129 grid, our data is obtained using a 41×41 grid ($Re = 100$), a 81×81 grid ($Re = 400$ and 1000), and a 161×161 grid ($Re = 3200$). In each case, our velocity profiles exhibit a perfect match with Ghia's results. In Fig. 2, we present similar data for larger values of the Reynolds number ($5000 \leqslant Re \leqslant 10000$). While

Table 4
Strength and location of the centers of tertiary vortex: bottom of the lid-driven square cavity

Re		Bottom left			Bottom right		
		ψ_{min}	x	y	ψ_{min}	x	y
3200	[6]	−6.33e − 8	0.0078	0.0078	−2.52e − 7	0.9844	0.0078
	Present	−3.74e − 8	0.0063	0.0063	−2.37e − 7	0.9875	0.0125
5000	[6]	−7.09e − 8	0.0117	0.0078	−1.43e − 6	0.9805	0.0195
	[5]	−2.33e − 7	0.0117	0.0098	−2.47e − 5	0.9668	0.0293
	[3]	−6.67e − 8	0.0079	0.0079	−1.43e − 6	0.9786	0.0188
	Present	−5.15e − 8	0.0063	0.0063	−1.70e − 6	0.9750	0.0188
7500	[6]	−1.83e − 7	0.0117	0.0117	−3.28e − 5	0.9492	0.0430
	[3]	−2.04e − 7	0.0112	0.0118	−3.28e − 5	0.9517	0.0422
	Present	−1.64e − 7	0.0063	0.0125	−1.89e − 5	0.9500	0.0375
10,000	[6]	−7.76e − 7	0.0156	0.0195	−1.31e − 4	0.9336	0.0625
	[3]	−1.13e − 6	0.0173	0.0201	−1.40e − 4	0.9351	0.0675
	Present	−8.64e − 7	0.0125	0.0187	−1.73e − 5	0.9563	0.0375

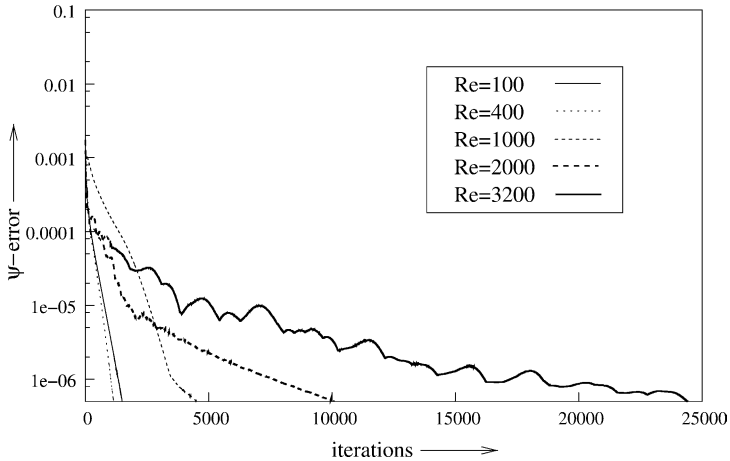

Fig. 7. Convergence history of the ψ-error for the lid-driven square cavity flow on a 41×41 grid on a PC with Pentium 4 processor and 256 mB RAM.

Table 5
Convergence data and relaxation parameter λ values for the lid-driven square cavity problem on a 41×41 grid on a PC with Pentium 4 processor and 256 mB RAM

Re	CPU (s)	Iterations	λ
100	30.086	1485	1.425
400	30.674	1155	1.025
1000	131.986	4096	0.500
2000	571.010	10,126	0.275
3200	724.445	24,413	0.125

Table 6
Strength and location of the centers of primary vortex for the rectangular lid-driven cavity flows with aspect ratio = 2

Re		100	400	1000	1500
Primary (Top)	[5]	−0.1033 (0.6172,1.7344)	−0.1124 (0.5547,1.5938)	−0.1169 (0.5273,1.5625)	– –
	Present	−0.1031 (0.6125,1.7375)	−0.1131 (0.550,1.6125)	−0.1182 (0.5250,1.5875)	−0.1189 (0.5250,1.5750)
Primary (Bottom)	[5]	7.83e − 4 (0.5391,0.5859)	9.09e − 3 (0.4297,0.8125)	0.0148 (0.3516,0.7891)	– –
	Present	5.232e − 4 (0.5625,0.6000)	8.021e − 3 (0.4375,0.8625)	0.0125 (0.3250,0.8750)	0.0140 (0.3498,0.8250)
Secondary (Bottom left)	[5]	−1.49e − 8 (0.0313,0.0313)	−2.57e − 7 (0.0391,0.0469)	−1.08e − 5 (0.0977,0.1094)	– –
	Present	−1.055e − 8 (0.0250,0.0375)	−2.8473e − 7 (0.0500,0.0500)	−6.7575e − 6 (0.1000,0.1250)	−9.221e − 5 (0.1750,0.2000)
Secondary (Bottom right)	[5]	−3.35e − 7 (1.0000,0.3750)	−1.46e − 7 (0.9688,0.0391)	−4.59e − 5 (1.0000,0.3750)	– –
	Present	−1.2073e − 8 (0.9750,0.0375)	−1.4215e − 7 (0.9500,0.0375)	−1.5687e − 7 (0.9600,0.0420)	−5.9117e − 7 (0.9375,0.0625)
Tertiary (Bottom left)	Present	– (–)	– (–)	– (–)	1.7793e − 9 (0.0125,0.0125)

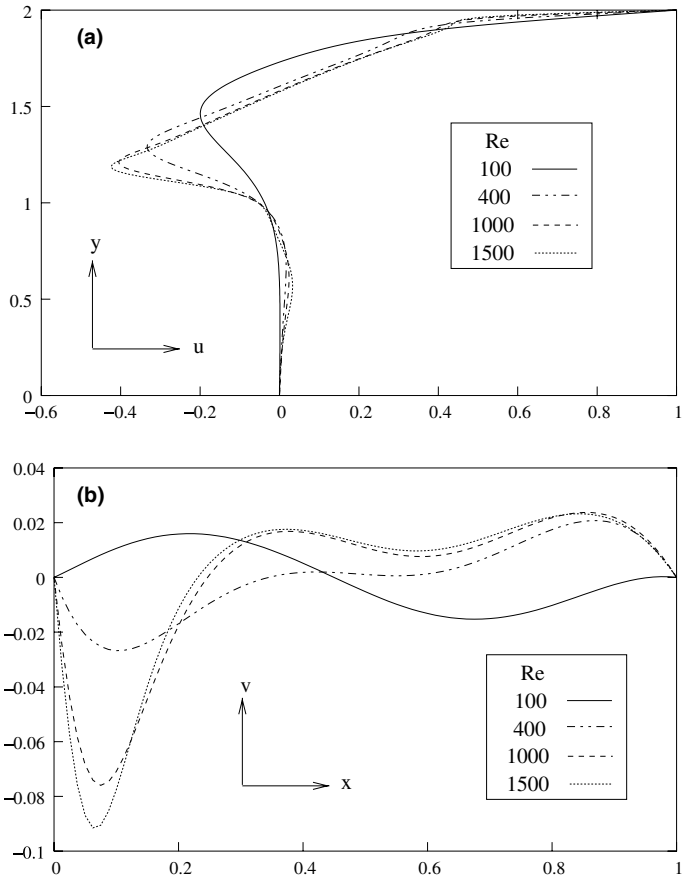

Fig. 8. (a) Horizontal velocity along the vertical centerline and (b) vertical velocity along the horizontal centerline for the rectangular lid-driven cavity flows with aspect ratio = 2 from $Re = 100$ to $Re = 1500$.

Ghia's results were obtained using 257×257 grids, we are able to obtain matching results with a 161×161 grid.

In Fig. 3, we exhibit the well known streamfunction contours for $100 \leqslant Re \leqslant 2000$ while Fig. 4 contains the corresponding contours for $3200 \leqslant Re \leqslant 10{,}000$. All of these graphs exhibit the typical separations and secondary vortices at the bottom corners of the cavity as well as at the top left of the square cavity. We also observe the evolution of tertiary vortices in the bottom corners of the cavity in Fig. 4. The tertiary vortices become quite visible for $Re = 5000$ and gain a significant size for $Re \geqslant 7500$. In Figs. 5 and 6, we exhibit the vorticity profiles for the range of the Reynolds numbers; these profiles are well known in the literature and exhibit no surprises thereby confirming the fact that our formulation yields qualitatively accurate solutions.

In Tables 1–4, we provide the quantitative comparison data for our solutions. In Table 1, we present the location of the center of the primary vortex and the value of streamfunction ψ at vortex center. This data is provided for $100 \leqslant Re \leqslant 10{,}000$ and available comparison data from the literature is also given in this table. In each case our solutions exhibit an excellent match with the best and most accurate solutions available in the literature. In Table 2, we present data on the secondary vortices ($100 \leqslant Re \leqslant 10{,}000$) in the bottom left and right corners of the square cavity. Again, our solutions exhibit an excellent match with the best

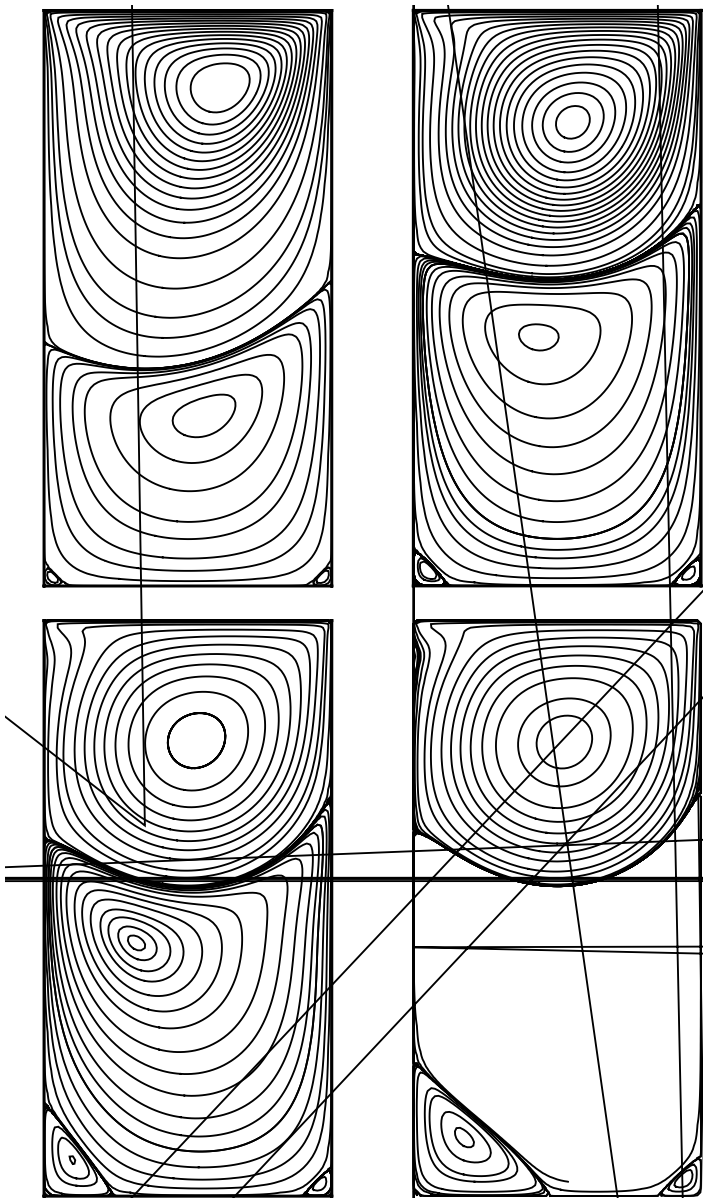

results in the literature. In Table 3, we present data on the secondary vortices on the left side wall near the top of the square cavity. This data is presented for $2000 \leqslant Re \leqslant 10{,}000$. While our results again exhibit an excellent match with the published results, we observe that our formulation allows us to detect the separation on the left side wall near the top of the square cavity for Reynolds numbers as small as $Re = 2000$. In Table 4, we present data on the tertiary vortices for $3200 \leqslant Re \leqslant 10{,}000$ and our results match very well with those in the literature.

In Fig. 7, we exhibit the convergence history of the ψ-errors on a 41×41 grid. As expected, the convergence for large Reynolds numbers requires larger number of iterations; in Table 5, we present the convergence data (and CPU time) for these cases. It is heartening to note that we were able to obtain the converged solutions for, e.g., $Re = 3200$ on a PC (with Pentium 4 and 256 mB RAM) in about 12 min of computation time.

4.2. Test problem 2

We now consider the problem of a lid driven flow in a rectangular cavity with aspect ratio of 2; this is similar to the previous problem except for the aspect ratio. This problem is defined and solved in the rectangle $0 \leqslant x \leqslant 1$, $0 \leqslant y \leqslant 2$. We solved this problem for Reynolds numbers Re ranging from 100 to 1500. This problem was earlier solved by Bruneau and Jouron [5] and we provide comparison data from their study in Table 6.

In Fig. 8, we exhibit the graphs of horizontal velocity along the vertical centerline and vertical velocity along the horizontal centerline for $100 \leqslant Re \leqslant 1500$. Fig. 9 contains the streamfunction contours for this problem for $100 \leqslant Re \leqslant 1500$. In each of these cases, we observe two rotating primary vortices as well as secondary vortices in the bottom corners of the rectangular cavity. There is also a tertiary vortex in the case of $Re = 1500$ though this vortex is not clearly visible in Fig. 9(d). In Table 6, we present quantitative data on the vortex center locations and the strength of primary, secondary and tertiary vortices for $100 \leqslant Re \leqslant 1500$; comparison data from [5] is also presented in this table.

We note further that Bruneau and Jouron [5] computed this problem for $Re \leqslant 1000$ and expected the steady flow to become turbulent for Reynolds numbers close to 1000. In our computations, we found the flow to stay laminar even at $Re = 1500$; our formulation allows us to obtain accurate converged solutions for this problem for $Re \leqslant 1500$.

5. Conclusions

In this paper, we introduce a new paradigm for solving the incompressible Navier–Stokes equations. Our formulation uses streamfunction and velocity as variables and avoids the difficulties traditionally faced with the primitive variables formulation and with streamfunction–vorticity formulation. Our formulation is used to solve several fluid flow problems and enables us to obtain high accuracy solutions with great efficiency. The present formulation has truncation error of second order; a fourth order method is presently being examined and results would be presented in future. We have had success with the use of multigrid technique in conjunction with this formulation for the Stokes flow ($Re = 0$) [1]. We are currently working to extend the multigrid technique to fluid flow problems for larger values of Reynold's numbers.

References

[1] I. Altas, J. Dym, M.M. Gupta, R. Manohar, Multigrid solution of automatically generated high-order discretizations for the biharmonic equation, SIAM J. Sci. Comput. 19 (1998) 1575–1585.
[2] I. Altas, J. Erhel, M.M. Gupta, High accuracy solution of three-dimensional biharmonic equations, Numer. Algorithm 29 (2002) 1–19.
[3] E. Barragy, G.F. Carey, Streamfunction–vorticity driven cavity solution using p finite elements, Comp. Fluid 26 (1997) 453–468.
[4] O. Botella, R. Peyret, Benchmark spectral results on the lid-driven cavity flow, Comp. Fluid 27 (1998) 421–433.
[5] C.-H. Bruneau, C. Jouron, An efficient scheme for solving steady incompressible Navier–Stokes equations, J. Comput. Phys. 89 (1990) 389–413.
[6] U. Ghia, K.N. Ghia, C.T. Shin, High *Re*-solution for incompressible Navier–Stokes equation and a multigrid method, J. Comput. Phys. 48 (1982) 387–411.

[7] M.M. Gupta, Discretization error estimates for certain splitting procedures for solving first biharmonic boundary value problems, SIAM J. Numer. Anal. 12 (1975) 364–377.
[8] M.M. Gupta, L.W. Ehrlich, Some difference schemes for the biharmonic equation, SIAM J. Numer. Anal. 12 (1975) 773–790.
[9] M.M. Gupta, R. Manohar, Direct solution of biharmonic equation using noncoupled approach, J. Comput. Phys. 33 (1979) 236–248.
[10] S. Hou, Q. Zou, S. Chen, G. Doolen, A. Cogley, Simulation of cavity flows by the lattice Boltzmann method, J. Comput. Phys. 118 (1995) 329–347.
[11] C.T. Kelley, Iterative Methods for Linear and Nonlinear Equations, SIAM Publications, Philadelphia, 1995.
[12] J. Kim, P. Moin, Application of fractional step method to incompressible Navier–Stokes equation, J. Comput. Phys. 59 (1985) 308–323.
[13] Y. Kwon, R. Manohar, J.W. Stephenson, Single cell fourth order methods for the biharmonic equation, Congres. Numerantium 34 (1982) 475–482.
[14] G. Meurant, Computer Solution of Large Linear Systems, North-Holland, Amsterdam, 1999.
[15] Y. Saad, Iterative Methods for Sparse Linear Systems, PWS Publishing Company, 1996.
[16] R. Schreiber, H.B. Keller, Driven cavity flows by efficient numerical techniques, J. Comput. Phys. 49 (1983) 310–333.
[17] G.L.G. Sleijpen, H.A. van der Vorst, Hybrid biconjugate methods for CFD problems, in: M. Hafez, K. Oshima (Eds.), Computational Fluid Dynamics Review, 1995, pp. 457–476.
[18] J.W. Stephenson, Single cell discretizations of order two and four for biharmonic problems, J. Comput. Phys. 55 (1984) 65–80.
[19] H. van Der Vorst, BiCGSTAB: a fast and smoothly converging variant of BiCG for the solution of nonsymmetric linear systems, SIAM J. Sci. Comput. 13 (1992) 631–644.
[20] S.P. Vanka, Block-implicit multigrid solution of Navier–Stokes equations in primitive variables, J. Comput. Phys. 65 (1986) 138–158.